Discretely assembled walking machines

Discretely Assembled Walking Machines

Cite this article as: Will Langford, Neil Gershenfeld, Discretely Assembled Walking Machines, *Journal of Micro-Bio Robotics*, doi: *10.1007/s12213-020-00128-1*

Discretely Assembled Walking Machines

Will Langford[1*] & Neil Gershenfeld[1]

[1] The Center for Bits and Atoms, Massachusetts Institute of Technology

Cambridge, MA – USA

[*] corresponding email: will.langford@cba.mit.edu

Submitted: October 4, 2019

Abstract: We introduce a discrete approach to robotic construction that enables the integration of structure, mechanism, and actuation and offers a promising route to on-demand robot fabrication. We demonstrate this with the assembly of two centimeter-scale electromechanical systems: a Discretely Assembled Walking Motor (DAWM) capable of producing large scale linear or rotary motion from five millimeter-scale part types as well as a Modular Tiny Locomoting Element (MOTILE) that can locomote on a variety of ferrous surfaces. The five part types each embody a limited capability including rigid (strut and node), flexural, magnetic, or coil. Through their arrangement in a three-dimensional lattice, we demonstrate the assembly of actuated mechanical degrees-of-freedom in useful small-scale machines. This work extends prior research in discrete material systems with the inclusion of flexural and actuation components. Actuation is accomplished with the use of voice coil actuator components that produce up to 42 mN of force and strokes of 2 mm. This performance compares well with other millimeter scale actuators and provides sufficient force to lift 28 connected nodes in our assembled lattice, or 7 other actuator components. DAWM is capable of stepping at rates of up to 35 Hz, resulting in velocities of up to 25 mm/s. Multiple DAWM systems can be stacked to add force and can be driven in-phase or out-of-phase to produce intermittent or continuous force, respectively. MOTILE can climb vertical surfaces at speeds of 2.46 body-lengths per second, representing the fastest vertical climbing robot in recently reported research. This approach to robot fabrication discretizes robotic systems at a much finer granularity than prior work in modular robotics and demonstrates the possibility of assembling useful small-scale machines from a limited set of standard part types.

Keywords: discrete assembly, electromagnetic, mobile, fabrication, assembly

Acknowledgements: This work was funded by Army Research Office (ARO) award W911NF-16-1-0568, and the Center for Bits and Atoms consortium.

INTRODUCTION

The design and fabrication of robots today can be expensive, inflexible, and time-consuming, often requiring the integration of a variety of parts, each made using separate and unrelated processes and with no standard assembly interface. The assembly and integration of these parts often represents a bottleneck in both the time and flexibility of the fabrication of a novel robotic system and as a result, recent research has looked for ways to fabricate robots in a more integrated way [1] [2].

This bottleneck is particularly present in the fabrication of millimeter-scale robotics where structure, mechanism, actuation, and control must be integrated very densely. Recent research in this field has looked to avoid the assembly and integration step altogether by fabricating devices in a single monolithic process. This includes processes that assemble intricate mechanisms through the lamination of various pre-machined layers [3][4][5], the integration of hydraulic channels in additively manufactured robot limbs [6], and even the direct printing of entirely soft robots [7]. However, each of these processes still has inherent limitations including the kinds of materials it can work with, the dimensionality of the end-product (2D vs 2.5D vs 3D), and the dynamic range it can support (maximum size per minimum feature size). As a result, no one process can span the full range of desired robotic capabilities.

Another way this assembly bottleneck has been addressed is with modular and reconfigurable components. Modular robotic systems integrate a number of capabilities such as actuation, communication, and control within every building block, enabling configuration and reconfiguration to suit a particular task. While these systems illustrate the universality of modular construction methods, the resulting modules tend to be relatively complex, involve dense integration of the various embedded functions, and are expensive to fabricate in volume [8]. As a result they have typically found limited use outside of the research lab.

Instead, the approach we introduce is based on discretely assembled "digital" materials. Digital materials are based on a discrete set of parts, which are reversibly joined with a discrete set of relative positions and orientations [9]. These properties allow global geometries to be determined from local constraints, assembly errors to be detected and corrected, heterogeneous materials to be joined, and disassembly and reuse rather than disposal [10]. Digital materials have been used to produce the highest reported modulus ultralight materials [11], shape morphing structures with the use of rigid and flexural parts [12], as well as electronic structures with the addition of conductive and insulating parts [13] [14].

We extend the space of digital materials here with the introduction of large-displacement flexural parts and actuation elements and demonstrate the assembly of electromechanical systems from just five part types. This approach builds systems with integrated structure, mechanisms, and actuation in a way that can be incrementally extended and modified. Standardizing the assembly interfaces between parts and simplifying the assembly process, to require just a single vertical motion, means the assembly process can more closely resemble a digital fabrication workflow. This ability to assemble integrated robotic systems from a small library of heterogeneous parts points towards the possibility for on-demand fabrication of a wide range of robots.

We demonstrate the assembly of long-range continuous motion from a small set of discrete parts by means of a Discretely Assembled Walking Motor (DAWM) and a Modular Tiny Locomoting Element (MOTILE) (Figure 1). The DAWM and MOTILE systems help answer questions about the viability of this assembly method for the fabrication of robotic systems and provides a test bed to quantify the performance of discretely assembled systems including the kinematics, dynamics, and coordination of multiple degrees of freedom.

In the following sections we detail the part and lattice geometry used as a basis for this work, the flexural parts that enable the assembly of mechanisms, the design and characterization of actuation elements, their integration in the DAWM and MOTILE systems, and the possibility to scale this approach to other length scales.

PART AND LATTICE GEOMETRY

We assemble digital material structures from repeated building block parts arranged in a rectangular lattice framework (Figure 1). Nodes of the lattice are assembled from four identical two-dimensional parts connected at

their edges. Nodes are connected by struts, which are either a simple two-dimensional part or a functional part such as a flexural degree-of-freedom or actuator.

The parts interlock through press-fit connections. The dimension of these slots is tuned to balance the force of insertion required during assembly with the mechanical and electrical reliability of the connection [13]. The parts are designed for automated assembly such that all of the interlocking connections are made in the vertical direction, enabling assembly with a simple single degree-of-freedom vertical motion.

The basic part types are two-dimensional so that they can be mass-produced in a range of materials and with a wide range of processes. While this assembly method may be applicable at a number of length scales, we have focused on the development of these parts at the millimeter scale. The parts shown here are 3.53 mm in their longest dimension, are 254 μm thick, and their smallest feature size is 200 μm (Figure 2).

By embedding degrees of freedom in the parts themselves, we can assemble mechanisms and linkages (Figure 3). Flexural parts are fabricated using a multi-layer laminate technique referred to as PC-MEMS (printed circuit MEMS) or SCM (smart composite microstructures) [3], [15], [16]. This technique enables the fabrication of hinges that are highly compliant about the hinge-axis but stiff off-axis. In this way, the flexural hinges act similarly to conventional macroscopic pin-joints but have the advantage of having virtually no backlash about their axis of rotation.

The flexural parts are made from layers of brass (100 μm thick) and Kapton (25 μm thick), and joined with two layers of B-staged Pyralux adhesive (12.5 μm thick) as pictured in Figure 2. This construction produces a hinge joint that is much more compliant about its rotation axis (28.9 mNmm/rad) than off-axis (9700 mNmm/rad). Similarly, a parallelogram linkage assembled from two degree-of-freedom struts measures 36.3 N/m on-axis and 6600 N/m off-axis.

Actuator Component Design and Characterization

At the millimeter scale, a number of actuation techniques can be used to drive these mechanisms, including piezoelectric bending actuators [17], dielectric elastomer actuators [18], shape-memory alloy actuators [19], and electromagnetic actuators [20].

We use electromagnetic Lorentz force (voice coil) actuation for its ability to produce constant force over long ranges. Electromagnetic actuators are used extensively at macro-scales but are less common at smaller scales because of energy-density scaling. However, considering improved current capacities at smaller scales and with the use of permanent magnets, use of electromagnetic actuators can be extended down to smaller sizes [21]. Relative to other electromagnetic actuators, Lorentz force actuators are able to produce a constant force (proportional to current) over a longer stroke and at a high-bandwidth. Additionally, there is no attractive force between the magnet core and coil, which reduces the demands on the mechanisms that constrain the coil's motion.

The actuator components span two cells of the lattice geometry and is pictured in Figure 4. This reduces the volumetric overhead associated with the integration of the coil and the magnetic core and means the force producing components can take up a larger portion of the overall volume. We designed the actuators to maximize their force over a 2 mm stroke. Like all other parts in this assembly system, the actuator components are designed to be vertically assemble-able and interface with the lattice using the same press-fit connections. Additionally, while the actuator components are more geometrically complex than the basic structural parts, they are still designed to be relatively easily mass produced. Coils of this size are regularly produced in large quantities, relatively inexpensively using surface mount inductor coil production techniques [22]. For prototyping we fabricate the parts using laminate methods, wire EDM, and semi-automated coil winding (Figure 2).

We modeled the actuator component using both magnetic circuit analysis and COMSOL multiphysics simulation software and verified this modeling with the physical testing detailed below. The static and dynamic performance of the actuator component is summarized in Table 1.

Table 1. Characteristics of the Actuator Component.

Coil Turns	75
Max. Continuous Current	0.6 A

Max. Continuous Current Density	24.2 A/mm^2
Force (blocked mid-stroke)	42 mN
Stroke (no load)	2.1 mm
Resonance (incl. parallelogram linkage)	75 Hz
Overall Mass	511 mg
Energy Density	89 J/g

Static Characterization

We tested the actuators both statically and dynamically. During static testing, we varied the current through the actuator coils and measured the resulting output force. The results show that the force of the actuator is linear with current and closely matches both analytical and numerical simulations (Figure 4). Because the models do not account for static friction or irregularities in the winding of the coil, they tend to over-predict the performance of the actuator. The analytical model also neglects leakage flux, which is unrealistic given the size of the air gap in the actuator. This model is described in more depth in Appendix A.

In Figure 4, beyond 700 mA, the actuator force becomes sublinear with current. This is likely a result of high temperatures in the coil affecting the effective flux density supplied by the magnets. We take 600 mA as the actuator's maximum steady state operating current, at which it reaches a temperature of 67 °C and produces an output force of 42 mN. Taking into account the cross-sectional area of a single wire turn, this represents a current density of 24.2 A/mm^2, which is more than two times greater than the recommended maximum current density for macroscopic electromagnetic actuators [23]; this is possible because of the relative scaling of surface area and volume, which allows better heat transfer out of the coil [21]. The 42 mN of output force is enough to lift 28 nodes of the lattice or 7 other actuator components, which is sufficient to produce useful motions and forces in discretely assembled machines with multiple degrees of freedom.

Dynamic Characterization

To measure the dynamic performance of the actuator, we supply a pseudo-random voltage to the actuator and use a high-speed camera to measure its response. The coil component of the actuator is rigidly fixed while the magnetic component is constrained by an assembled parallelogram flexure linkage, which approximates linear motion for small displacements. Dividing the frequency response of the output displacement by that of the input voltage, results in the transfer function that describes how the output relates to the input over a range of frequencies. This data, presented in Figure 4, is described well by a second-order spring mass damper model with a 75 Hz natural frequency and a quality factor of 6.2. This model is useful in predicting the performance of the actuated system over a range of frequencies and gives an estimate of the bandwidth of the actuator and flexure combination.

Comparison to other millimeter-scale actuators

The actuator component developed here compares well against other millimeter-scale actuators that have been recently reported in research. We compiled data regarding actuator force, mass, stroke, and bandwidth and plot the normalized actuator force (per weight) against maximum stroke (Figure 5). Wherever possible we include the mass of the whole actuator (stator and mover) as well as the mass of the motion constraint. The actuator component developed in this work has the highest normalized force (blocked force per weight) of any of the comparably sized electromagnetic actuators presented here [16] [20]–[24]. Piezoelectric [13] [25] and electrostatic [26] [27] actuators produce more force per mass but are more limited in their available stroke. We discuss possible methods to increase the performance of the actuator in the conclusion.

SYSTEM INTEGRATION

We built a Discretely Assembled Walking Motor (DAWM) and a Modular Tiny Locomoting Element (MOTILE) to demonstrate the integration of structure, mechanism, and actuation.

DAWM – Discretely Assembled Walking Motor

The DAWM system takes small cyclical steps to produce long range motion of a sliding or rotating element. This principle of locomotion is most commonly used with piezoelectric actuators [29] for applications such as nanometer-precision stages [30] and focusing motors in DSLR cameras [31]. Here, we use the voice coil actuator components developed for our assembled structures to enable the same kinds of motion with larger displacements and lower voltages.

The DAWM system is composed of five part types: structural nodes, rigid and dual-hinged struts, and magnetic and coil part types (Figure 1). The two actuator components are oriented perpendicularly to one another and the output of the actuators is coupled to a motor tip through multiple four-bar parallelogram linkages, which distribute the two degrees of freedom at the tip into a single degree of freedom at each actuator. As the motor tip is driven cyclically, it engages with a grooved sliding or rotating element. In our design, the motor tip consists of a 0.5 mm cylinder which provides quasi-kinematic mating with the triangular grooves of the rotor. The triangular grooves are spaced 0.75 mm apart and correspond to a segment of the approximately circular trajectory of the motor tip. This geometry is designed to allow for the correction of motor-tip positioning errors within +/-0.15 mm. The motor works with a variety of different surfaces including ones that are smooth; however, the grooved surface employed here provides the highest repeatability.

Speed and Repeatability

We characterize the repeatability of the walking motor across a range of stepping frequencies, by taking 10 steps at each frequency and computing the average velocity at each. We sweep the frequency up and down, increasing and decreasing the step rate a number of times, to get a sample size of six at each tested frequency.

The results (Figure 6) show good agreement to the predicted performance. Below 12 Hz, the difference between measured and predicted velocities is negligible. Between 12 Hz and 34 Hz, there is more variability in the relationship between step frequency and velocity with the largest standard deviation being 25% of the mean. However, the overall slope remains consistent with our predictions. This indicates that at the higher step-rates the motor is just as likely to take a double-step as it is to miss a step. We hypothesize that step variability occurs because the motion amplitude increases as the step-rate approaches the resonant frequency of the walking motor and causes the motor to occasionally skip a tooth. Beyond 35 Hz the velocity drops dramatically as the steps become very erratic and intermittent, indicating a maximum open loop speed of approximately 25 mm/s.

Force Additivity

To characterize the effects of phasing multiple walking motors, we measured the blocked force of a stacked two-layer walking motor while driving at a 1 Hz step rate to ensure sufficient resolution to resolve the full force profile (Figure 6).

When the two motors are driven in phase, their peak force is approximately twice (70 mN) that of the single motor (30 mN). When the two motors are driven out of phase, they produce a more uniform force which varies between 20 mN and 50 mN. The magnitudes of these forces are on par with the maximum blocked force of the individual actuators themselves. In the single motor case, 79% of the maximum blocked force of a single actuator is translated to the rotor at its peak force. In the two-motor case, 92% of the maximum blocked force of two single-actuators is translated to the rotor at its peak force.

MOTILE – Modular Tiny Locomoting Element

The MOTILE system converts repeated small displacement steps into long range locomotion. MOTILE is assembled from the same five part types as the DAWM system with an additional “foot” part-type that enables the walking machine to attach and detach from a surface.

An Electropermanent Foot

A number of different physical mechanisms can be used to selectively and controllably attach and detach from surfaces including electromagnetism [32], electroadhesion [33], dry adhesion [34], and tunable microstructure [35]. In this work, we use a particular kind of electromagnetic actuator that is often referred to as an electropermanent magnet.

Electropoermanent actuators are magnets that can be switched on and off with a short pulse of current and have been shown to work effectively in small scale robotic systems ([31] [32] [38]). The advantage of electropermanent actuators over conventional electromagnets is that they hold their state with no current and so are far more energy efficient when operated at low frequencies. Additionally, because the magnets in an electropermanent actuator represent a high reluctance path, electropermanent actuators are far less sensitive to large air gaps between the actuator and the surface than a conventional electromagnet is (Figure 7). We had initially tested making a MOTILE with electromagnets rather than electropermanent magnets and found that the attractive force was highly sensitive to very small air gaps between the foot and the surface. This manifested in the MOTILE being very sensitive to the orientation of the wires that were providing power to the actuators. A MOTILE using electropermanent feet does not suffer from this same sensitivity.

The shear force exerted by the electropermanent actuator in its on and off state varies with the pulse voltage (and current). We tested the shear force at a number of different voltage levels from 10 V to 16 V using a fixed pulse duration of 300 μs (Figure 7). In performing the test, the actuator is placed on a ground steel surface and an aluminum post is used to couple the actuator to the load cell. The steel surface is advanced towards the loadcell and the maximum force seen by the loadcell is recorded. This provides a measure of the dynamic friction between the ground steel surface and the actuator. The test indicates that the magnitude of the current pulse determines the strength of the foot attachment. It's clear that a greater difference between the "on" and "off" state is achieved for higher pulse voltages. At 16 V (the maximum voltage permitted by the H-bridge in use) there is a roughly 20x increase in shear force between the "on" and "off" states. We also measured the normal force exerted by this actuator. On a ground steel surface the normal force measures 2.23 ± 0.24 N (n=6), when activated. This is enough force to support the weight of over 400 actuator components (511 mg).

Characterization

The walker, MOTILE, is assembled from six part types: rigid struts, rigid nodes, 2-DoF struts, a magnetic part, a coil part, and electropermanent feet. A central Lorentz force actuator provides the motive force and the relative order of when the electropermanent feet are switched determines the direction of motion.

We tested the MOTILE on a number of different ferromagnetic surfaces including ones with a thin layer of lower friction material (polyimide) but ultimately found the best performance when the electropermanent feet were in direct contact with a ferrous surface. We also found that adding a small plastic spring helped accentuate the difference in friction of the on and off states of the feet and was beneficial for consistent locomotion. These two springs (one per electropermanent foot) have the effect of reducing the friction between the unlatched foot and the surface without significantly affecting the friction force of the latched foot and the surface.

In addition to testing a range of different surface materials, we also tested the robot in a number of different orientations. Because the potential shear force ($>$0.4 N) and the normal force (2.2 N) of the feet are both much greater than the weight of the robot ($\approx$0.02 N), the robot is able to walk up vertical walls as well as upside down on inverted surfaces (Figure 8).

We used motion tracking software (Tracker) to measure the speed of the MOTILE in a variety of orientations. In analyzing the speed of the walker as it climbs a vertical ground steel block, the walker takes a trajectory that's roughly 60-degrees from horizontal. The MOTILE is driven at approximately 45 Hz. The speed is consistent and measures approximately 36.2 mm/s going up and 44.2 mm/s going down. Doing the same on a flat surface, we measure an average speed of 37 mm/s over 5 trials.

To compare this performance to other robots in recently reported research, we normalize the speed by dividing by the length of the robot to get a measure in terms of body-lengths per second (BL/s). Given its 15 mm body length, the MOTILE climbs up the block at 2.4 BL/s and down at 2.95 BL/s. It moves on a flat surface at 2.46 BL/s. Comparing these values to others reported in recent literature reveals that this robot is the fastest vertical climbing

robot (Figure 9). This being said, there are certainly a number of caveats and limitations to consider. For one, MOTILE is driven entirely off-board by external control electronics and as such carries less weight than robots that are untethered. Another severe limitation of this robot is the need for a ferromagnetic surface. However, this is certainly not the only robot to use magnetic forces for climbing and others have argued that many desirable applications for mobile climbing robots would be satisfied with the use of magnetic forces [39] [40] [41] [42].

DISCUSSION

We have shown that machines with integrated mechanisms and actuation can be assembled from a small set of building blocks. In particular, we developed six part-types that enable the assembly of a walking motor, which converts small displacement cyclical motion into precise long range linear and rotary motion at up to 25 mm/s, and a walker capable of climbing up ferrous surfaces at up to 36.2 mm/s (2.4 BL/s). We showed that by embedding flexural hinges in the part set, we can assemble compliant mechanisms that have high ratios of on- to off-axis compliance. Furthermore, we developed an actuator component, integrated in the same assembly framework, that produces enough force to lift seven times its own mass.

Scaling

While we have focused development at the millimeter-scale, other application domains may be possible by scaling the constituent parts and assemblies. For example, with smaller micro-scale building block parts, applications requiring finer-grain resolution can be explored such as ingestible medical robots and dexterous microsurgical tools.

It is possible to project the performance of these assemblies to other length scales through a proportionality scaling analysis (Table 2). We use the scale variable, s, to represent how a particular quantity scales, as is detailed in [43]. In our case, as we scale the stroke of the actuator down (s), we assume that the actuation current can scale with a constant temperature rise (s^1), rather than constant current density (s^2), because surface area scales favorably with respect to volume. Based on this assumption, both power and force (as well as their respective densities) scale favorably to smaller length-scales. Furthermore, bandwidth also scales favorably, proportionally increasing for every shrink in size. Efficiency, however, suffers at smaller length scales and decreases proportionally with scale.

Table 2. Scaling Laws for Voice Coil Actuation

Mass	s^3	Power	s^2
Current	s^1	Power Density	s^{-1}
Force	s^2	Force Density	s^{-1}
Bandwidth	s^{-1}	Efficiency	s^1
Energy Output	s^3	Energy Density	s^0

This points to the possibility of scaling this assembly approach down in length-scale. At some-point, however, the increase in bandwidth, force, and power density will be outweighed by the decrease in efficiency and will warrant a different type of actuation (for example, piezoelectric or electrostatic). Furthermore, this theoretical analysis neglects practical constraints which surely become important as the scale in increased or decreased dramatically. These include, for example, the dimensionality, tolerance, and surface finish that can be achieved with micro- and meso-scale fabrication methods.

Assembly at smaller length scales is often complicated by decreased positioning accuracy and difficulties in part manipulation because of the scaling of surface forces relative to inertial ones. We expect our discrete assembly method to be more amenable to high throughput assembly at small scales because the assembly accuracy comes from the interlocking geometry of the parts, rather than a global positioning system, and the part-part interlocking forces can be tuned to enable reliable part placement. Prior work has shown that the degree of positioning error tolerance can be as high as 39% of the part spacing [13].

Limitations and Opportunities

The maximum frequency of the DAWM system is 35 Hz and is limited, in part, by the electronic drive circuitry. The actuator uses 34-awg wire, resulting in a low inductance coil (15 μH) that experiences current ripple losses when driven directly by an H-bridge with insufficiently high frequency PWM (1 kHz, in this case). Decreasing the wire diameter to 40-awg and increasing the PWM frequency to 31.25 kHz would reduce the current ripple by 88% and the resulting dissipation by 70%, potentially enabling actuation rates up to the 75 Hz bandwidth of the actuator-flexure combination.

The actuation rate could be further increased by stiffening the flexure degrees-of-freedom. Our flexures were designed to be highly compliant to enable long strokes to suit a wide variety of applications. Given the electrical time constant of the actuator coils ($\tau = L/R = 100\mu s$), actuation rates of several hundreds or thousands of cycles per second should be possible at the expense of the actuator stroke. While the DAWM system has not been tested to fatigue, prior research has shown that the flexural hinges used here can be made to survive millions of cycles before failure [44].

While we've demonstrated the assembly of a single degree-of-freedom walker, MOTILE, that can only move forward or backward, these modules could be composed to build positioning devices with the ability to move in multiple directions. Two MOTILE's placed side-by-side could be used to move forward and backward as well as turn left and right. Four MOTILE's arranged in a cross-shaped circular array could be used to translate in any direction as well as rotate about the plane.

The motion of an individual MOTILE relies on a friction interface with the surface and so the exact size and direction of each step can vary from step to step. This results in motion that is sometimes not perfectly straight or that varies in speed (for example, climbing up versus down the steel block). It would be beneficial to eliminate these sources of uncertainty in order to build machines that can position precisely and repeatably without requiring an additional sensing mechanism. This could be accomplished with the use of a structured surface that attracts each step to a potential minimum. This structuring could be done with a physically grooved surface or by structuring permeability (as is done in a linear stepper motor).

In both of these assemblies, power has been supplied externally from benchtop power supplies. Future work should involve incorporation of mobile on-board power sources to enable truly mobile robots. Zinc-air batteries have among the highest energy densities of battery technologies. These batteries are commonly used in hearing aids and are designed to provide energy for a low draw (a few milliamps) for a week or more. While they have great energy densities, zinc-air batteries are not rechargeable and expire with or without use in a few weeks time (after the tab is removed and air is let in). A size 10 battery (the smallest commonly available hearing aid battery) is 5.8 mm x 3.6 mm. Two of these could be stacked to fit on a single actuator sized building block that spans two cells of the lattice (taking up a volume roughly 5 mm x 9 mm x 4 mm). This would provide approximately 200 mAh of capacity, enough to power a single actuator, which draws 100 mA (the 320-turn coil), for two hours. An individual MOTILE would be capable of carrying the weight of this battery, albeit with a slower vertical climbing speed.

The regularity of the geometry in these assemblies lend themselves well to automated assembly. The work shown here was manually assembled, however prior work has shown the possibility of automating the assembly in a desktop process [14]. Prior assembly systems in this category have been able to leverage the interlocking nature of the discrete parts to assemble structures with a high degree of error tolerance [13]. Additionally, we have not included discussion of methods to integrate circuitry, controls, and power storage within the same assembly framework. Prior work has shown the possibility of assembling circuitry, including active electronics in similar assembly systems [13] [14]. Based on this, future work will involve the assembly of integrated robotic systems such as grippers, micro-positioners, and mobile robots with onboard power and control.

In the same way that computers and digital technology rest on the ability of a small family of gates to evaluate arbitrary logical expressions [45], this work points to a small family of building blocks that enable the construction of arbitrary robotic capabilities. While the design and fabrication of robots today often requires the integration of many diverse and custom parts, by standardizing the part set through the development of discrete assembly workflows, we can take advantage of the same benefits inherent in computational universality and enable more flexible, inexpensive, and rapid design of robotic systems. The results reported here show the utility of even a

limited standard part set and the opportunity for future work to extend the part set to encompass a full range of robotic capabilities.

REFERENCES

[1] S. Tibbits, "From Automated to Autonomous Assembly," *Archit. Des.*, vol. 87, no. 4, pp. 6–15, 2017.

[2] J. Paik, "Soft robot design methodology for 'push-button' manufacturing," *Nat. Rev. Mater.*, pp. 1–3, 2018.

[3] J. P. Whitney, P. S. Sreetharan, K. Y. Ma, and R. J. Wood, "Pop-up book MEMS," *J. Micromechanics Microengineering*, vol. 21, no. 11, p. 115021, 2011.

[4] A. T. Baisch and R. J. Wood, "Pop-up assembly of a quadrupedal ambulatory MicroRobot," *IEEE Int. Conf. Intell. Robot. Syst.*, pp. 1518–1524, 2013.

[5] H. McClintock, F. Z. Temel, N. Doshi, J. Koh, and R. J. Wood, "The milliDelta: A high-bandwidth, high-precision, millimeter-scale Delta robot," *Sci. Robot.*, vol. 3, no. 14, p. eaar3018, 2018.

[6] C. Semini *et al.*, "A Brief Overview of a Novel, Highly-Integrated Hydraulic Servo Actuator with Additive-Manufactured Titanium Body," *IROS Work. 2016*, pp. 4–7, 2016.

[7] M. Wehner *et al.*, "An integrated design and fabrication strategy for entirely soft, autonomous robots," *Nature*, vol. 536, no. 7617, p. 451, Aug. 2016.

[8] Z. Butler and A. Rizzi, "Distributed and Cellular Robots," in *Springer Hanbook of Robotics*, 2008, pp. 911–920.

[9] G. A. Popescu, T. Mahale, and N. A. Gershenfeld, "Digital materials for digital printing," *NIP Digit. Fabr. Conf.*, pp. 1–4, 2006.

[10] J. D. Hiller and H. Lipson, "Fully Recyclable Multi-Material Printing," *Solid Free. Fabr. Symp.*, pp. 98–106, 2009.

[11] K. C. Cheung and N. Gershenfeld, "Reversibly Assembled Cellular Composite Materials," *Science (80-.).*, vol. 341, no. September, pp. 1219–1221, 2013.

[12] B. Jenett *et al.*, "Digital Morphing Wing: Active Wing Shaping Concept Using Composite Lattice-Based Cellular Structures," *Soft Robot.*, 2017.

[13] W. Langford, A. Ghassaei, and N. Gershenfeld, "Automated Assembly of Electronic Digital Materials," in *ASME MSEC*, 2016, pp. 1–10.

[14] R. MacCurdy, a. McNicoll, and H. Lipson, "Bitblox: Printable digital materials for electromechanical machines," *Int. J. Rob. Res.*, Jul. 2014.

[15] R. J. Wood, S. Avadhanula, R. Sahai, E. Steltz, and R. S. Fearing, "Microrobot Design Using Fiber Reinforced Composites," *J. Mech. Des.*, vol. 130, no. 5, p. 052304, 2008.

[16] N. Doshi *et al.*, "Model driven design for flexure-based Microrobots," in *IEEE International Conference on Intelligent Robots and Systems*, 2015, vol. 2015-Decem, pp. 4119–4126.

[17] R. J. Wood, E. Steltz, and R. S. Fearing, "Optimal energy density piezoelectric bending actuators," *Sensors Actuators A Phys.*, vol. 119, no. October 2004, pp. 476–488, 2005.

[18] A. P. Gerratt, B. Balakrisnan, I. Penskiy, and S. Bergbreiter, "Dielectric elastomer actuators fabricated using a micro-molding process," *Smart Mater. Struct.*, vol. 23, no. 5, p. 055004, May 2014.

[19] N. J. Kohut, A. M. Hoover, K. Y. Ma, S. S. Baek, and R. S. Fearing, "MEDIC: A legged millirobot utilizing novel obstacle traversal," *Proc. - IEEE Int. Conf. Robot. Autom.*, pp. 802–808, 2011.

[20] B. Goldberg, M. Karpelson, O. Ozcan, and R. J. Wood, "Planar fabrication of a mesoscale voice coil actuator," *2014 IEEE Int. Conf. Robot. Autom.*, pp. 6319–6325, 2014.

[21] W. Trimmer and R. Jebens, "Actuators for micro robots," *Proceedings, 1989 Int. Conf. Robot. Autom.*, pp. 1547–1552, 1989.

[22] Ingrid West Machinery Ltd., "Fully Automatic Hot Air Coil Winding Machine." [Online]. Available: http://coilwindingmachines.eu/automatic_winding_machines/hot_air_coil_winding_machine.html.

[23] D. C. Hanselman, *Brushless permanent magnet motor design*. 2006.

[24] C. S. Liu and P. D. Lin, "Miniaturized auto-focusing VCM actuator with zero holding current," *Opt. Express*, vol. 17, no. 12, p. 9754, 2009.

[25] M. Salerno, A. Firouzeh, and J. Paik, "A Low Profile Electromagnetic Actuator Design and Model for an Origami Parallel Platform," *J. Mech. Robot.*, vol. 9, no. 4, p. 041005, 2017.

[26] P. A. York, S. Member, R. J. Wood, and S. Member, "A geometrically-amplified in-plane piezoelectric actuator for mesoscale robotic systems," pp. 1263–1268, 2017.

[27] R. Yeh, S. Hollar, and K. S. J. Pister, "Single mask, large force, and large displacement electrostatic linear inchworm motors," *J. Microelectromechanical Syst.*, vol. 11, no. 4, pp. 330–336, 2002.

[28] E. W. Schaler, T. I. Zohdi, and R. S. Fearing, "Thin-film repulsive-force electrostatic actuators," *Sensors Actuators, A Phys.*, vol. 270, pp. 252–261, 2018.

[29] R. Merry, R. Van De Molengraft, and M. Steinbuch, "Modeling of a walking piezo actuator," *Sensors Actuators, A Phys.*, 2010.

[30] Physikinstrumente, "Piezo Walk Piezo Motors," 2018. [Online]. Available: https://www.physikinstrumente.com/en/technology/piezoelectric-drives/piezowalk-piezo-motors/.

[31] K. Spanner and B. Koc, "Piezoelectric Motors, an Overview," *Actuators*, vol. 5, no. 1, p. 6, 2016.

[32] L. Sun, P. Sun, C. Wang, and X. Qin, "Mobile micro-robot in small pipe driven by electro-magnetic force," *J. Shanghai Univ. (English Ed.)*, 2007.

[33] S. D. De Rivaz, B. Goldberg, N. Doshi, K. Jayaram, J. Zhou, and R. J. Wood, "Inverted and vertical climbing of a quadrupedal microrobot using electroadhesion," 2018.

[34] W. A. Breckwoldt, K. A. Daltorio, L. Heepe, A. D. Horchler, S. N. Gorb, and R. D. Quinn, "Walking inverted on ceilings with wheel-legs and micro-structured adhesives," *IEEE Int. Conf. Intell. Robot. Syst.*, vol. 2015-Decem, no. October, pp. 3308–3313, 2015.

[35] P. Birkmeyer, A. G. Gillies, and R. S. Fearing, "CLASH: Climbing vertical loose cloth," *IEEE Int. Conf. Intell. Robot. Syst.*, pp. 5087–5093, 2011.

[36] A. N. Knaian, "Electropermanent Magnetic Connectors and Actuators : Devices and Their Application in Programmable Matter," Massachusetts Institute of Technology, 2010.

[37] A. N. Knaian, K. C. Cheung, M. B. Lobovsky, A. J. Oines, P. Schmidt-Neilsen, and N. A. Gershenfeld, "The Milli-Motein: A self-folding chain of programmable matter with a one centimeter module pitch," *IEEE Int. Conf. Intell. Robot. Syst.*, pp. 1447–1453, 2012.

[38] K. Gilpin, A. Knaian, and D. Rus, "Robot pebbles: One centimeter modules for programmable matter through self-disassembly," *2010 IEEE Int. Conf. Robot. Autom.*, pp. 2485–2492, May 2010.

[39] Z. Bi, Y. Guan, S. Chen, H. Zhu, and H. Zhang, "A miniature biped wall-climbing robot for inspection of magnetic metal surfaces," *2012 IEEE Int. Conf. Robot. Biomimetics, ROBIO 2012 - Conf. Dig.*, pp. 324–329, 2012.

[40] X. Tang, D. Zhang, Z. Li, and J. Chen, "An omni-directional wall-climbing microrobot with magnetic wheels directly integrated with electromagnetic micromotors," *Int. J. Adv. Robot. Syst.*, vol. 9, 2012.

[41] M. Eich and T. Vogele, "Design and control of a lightweight magnetic climbing robot for vessel inspection," *2011 19th Mediterr. Conf. Control Autom. MED 2011*, no. June, pp. 1200–1205, 2011.

[42] G. Lee, G. Wu, J. Kim, and T. Seo, "High-payload climbing and transitioning by compliant locomotion with magnetic adhesion," *Rob. Auton. Syst.*, vol. 60, no. 10, pp. 1308–1316, 2012.

[43] W. S. N. Trimmer, "Microrobots and Micromechanical Systems," *Sensors and Actuators*, vol. 19, no. 3, pp. 267–287, 1989.

[44] R. Malka, A. L. Desbiens, Y. Chen, and R. J. Wood, "Principles of microscale flexure hinge design for enhanced endurance," *IEEE Int. Conf. Intell. Robot. Syst.*, no. Iros, pp. 2879–2885, 2014.

[45] C. E. Shannon, "A symbolic analysis of relay and switching circuits," *American Institute of Electrical Engineers, Transactions of the*, vol. 57, no. 12. pp. 713–723, 1938.

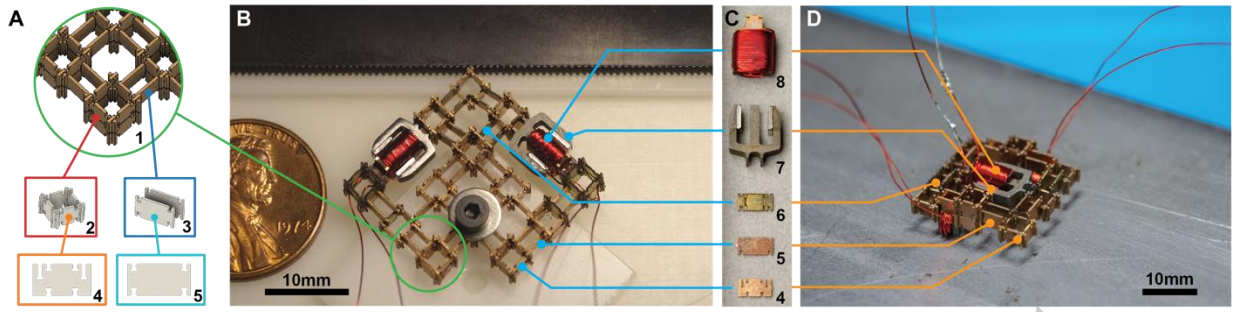

Figure 1. An overview of the walking machines assembled from five common part types. (A) The lattice decomposition into two-dimensional parts. Node parts (4) are first assembled into nodes (2) which are then connected with struts (5) arranged in parallel (3). (B) A discretely assembled walking motor (DAWM) configured to produce linear motion. (C) The five part include: node parts (4), rigid struts (5), dual-hinge struts (6), magnetic core (7), and voice coil (8). (D) A modular tiny locomoting element (MOTILE) assembled from the same part types.

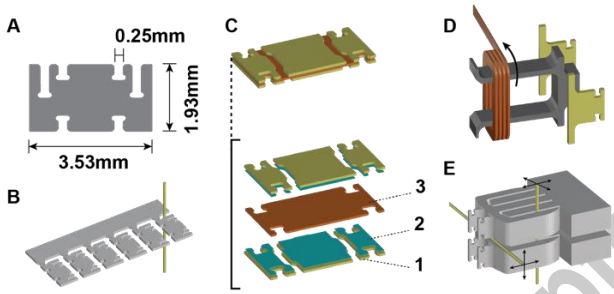

Figure 2. Part production techniques used in prototyping. Dimensioned node part (A) is cut with wire-EDM (B). Parts with flexural hinges (C) are fabricated by laminating layers of brass (1), B-staged adhesive (2), and Kapton (3). Coil parts are made by winding wire around a mandrel (D). Magnetic cores are made with two orthogonal wire-EDM cuts (E).

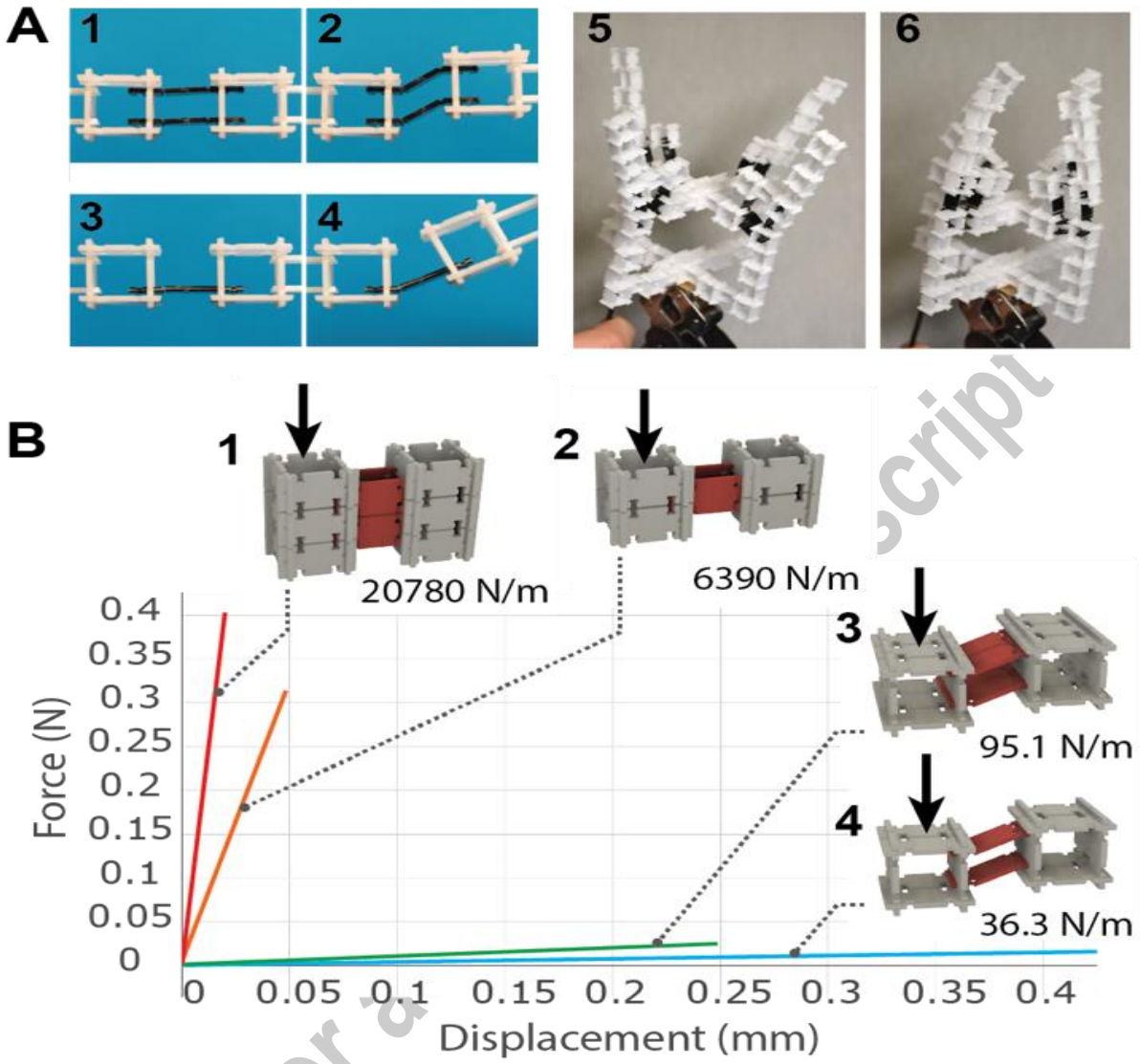

Figure 3. Mechanisms are assembled from parts with flexural degrees of freedom. Two common mechanism motifs (A) are parallelogram linkages (1)(2) and a single-hinge rotary joint (3)(4). These are combined to assemble a gripper (5)(6). The mechanisms exhibit a high degree of compliance on-axis while remaining stiff off-axis (B).

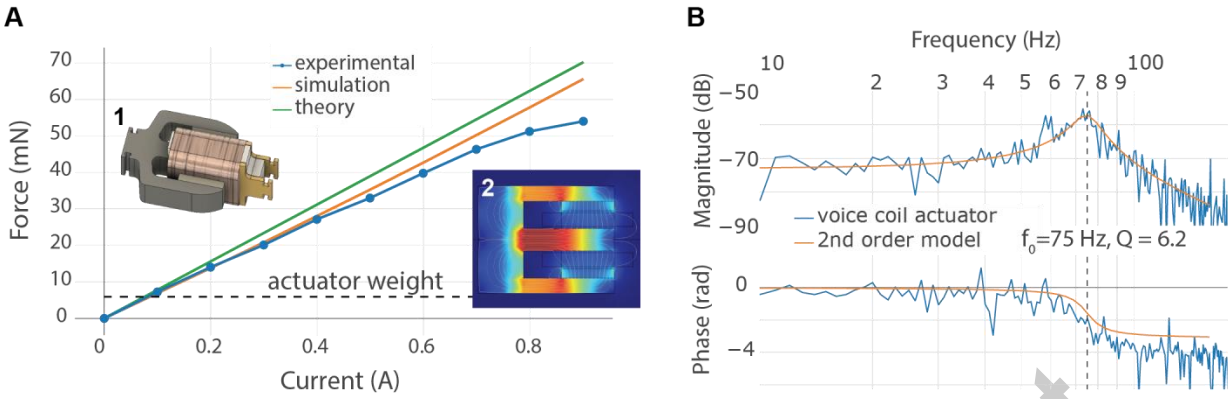

Figure 4. Actuator characterization. (A) The results of static testing and comparisons with theoretical and numerical modeling. (B) The results of dynamic testing showing a natural resonant frequency of the actuator and mechanism combination of 75 Hz.

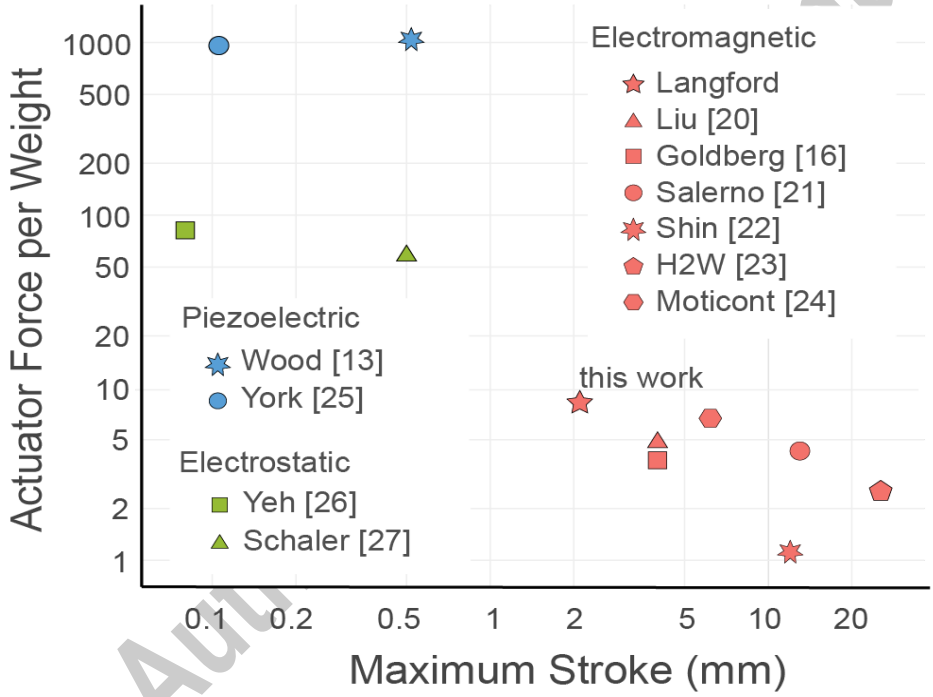

Figure 5. Comparison of normalized force versus stroke with other research and commercial millimeter-scale actuators.

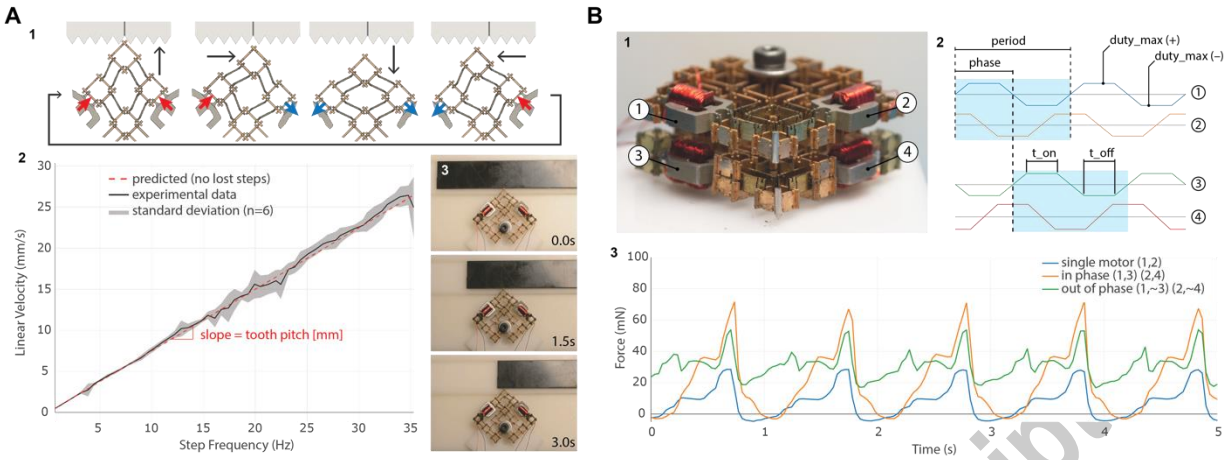

Figure 6. Walking motor characterization. (A) Speed and reliability testing done on a single-layer walking motor illustrates the series of steps during one actuation cycle (1) as well as the progression of a slider over three seconds (3) and the resulting velocity of the mover/rotor (2). The force output of the walking motor (B)(1) driven by a trapezoidal waveform (2) out-of-phase and in-phase (3).

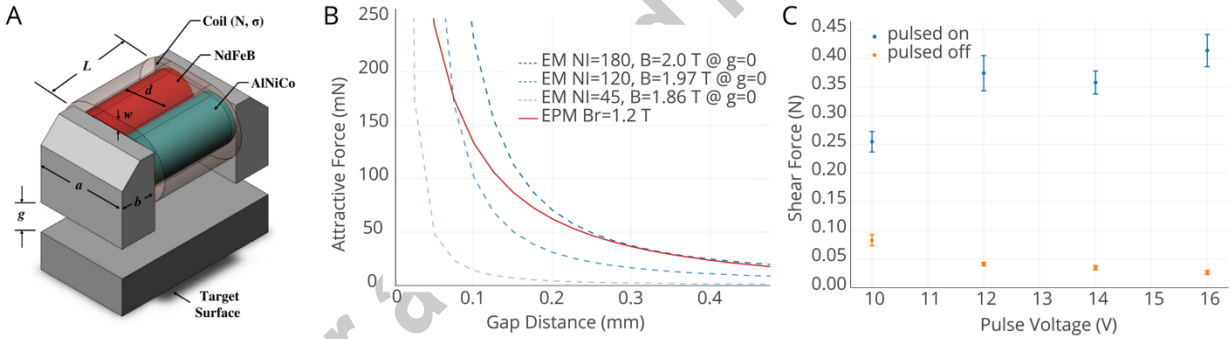

Figure 7. (A) Reproduced from [36]*. Construction of electropermanent magnet. (B) Plotting the attractive force across an airgap is plotted for electromagnets (EM) with varying magnetomotive forces (NI) against an electropermanent magnet with a given residual flux (Br) shows that electropermanent magnets are far less sensitive to large air-gaps and produce more attractive force than an equivalently sized electromagnet. (C) The degree to which the electropermanent actuator is switched can be controlled.*

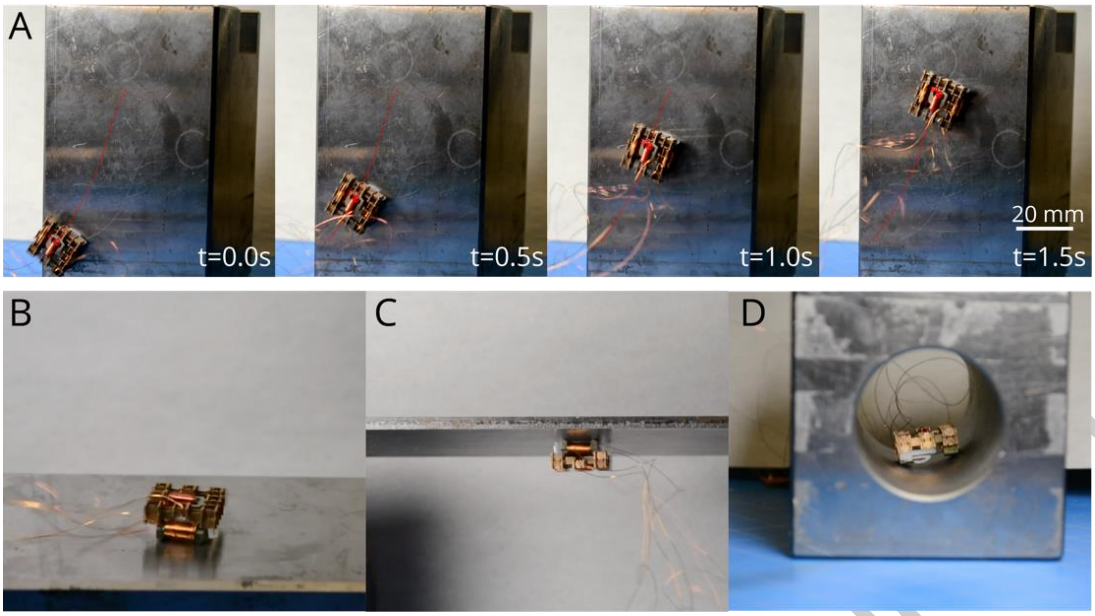

Figure 8. The walker is able to walk on surfaces of a variety of orientations including up vertical walls (A), on horizontal surfaces (B), upside down (C), and on non-flat surfaces (D).

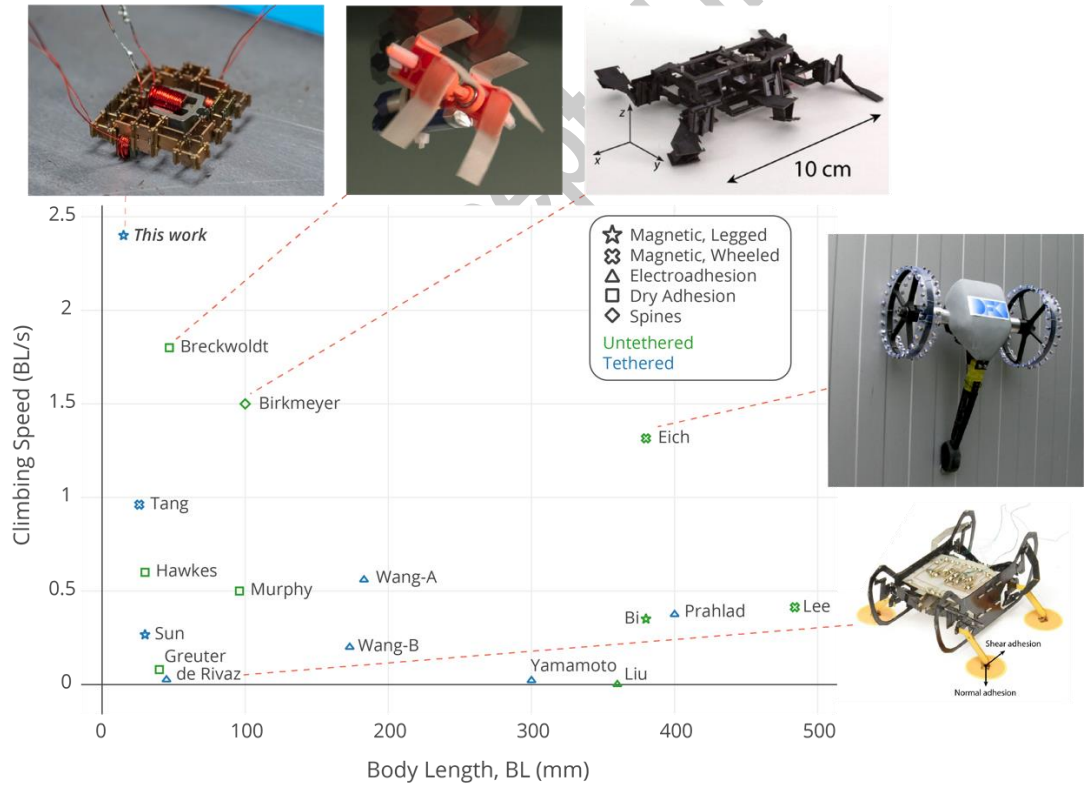

Figure 9. Comparing the climbing performance of the single degree-of-freedom MOTILE walker to other vertical climbing robots. MOTILE is both the smallest and fastest (in body-lengths per second) of any robot in recently reported research with the caveat that it is not able to turn and doesn't contain onboard power or control.